RUSSIAN ACADEMY OF SCIENCE
Lenin Order of Siberian Branch
G.I. BUDKER INSTITUTE OF NUCLEAR PHYSICS

V.I. Davydenko, A.A. Ivanov,
I.A. Kotelnikov, M.A. Tiunov

PIERCE ELECTRODES FOR A MULTIGAP ACCELERATING SYSTEM

Budker INP 2006-11

Novosibirsk
2006

V.I. Davydenko, A.A. Ivanov, I.A. Kotelnikov, M.A. Tiunov

Pierce electrodes for a multigap accelerating system

Institute of Nuclear Physics, 630090, Novosibirsk, Russia

Abstract

A well-known Pierce's solution [1, 2] that allows to focus a beam of charged particles using properly shaped electrodes outside of the beam is generalized to the case of multigap accelerating system. Simple parametric formulae for Pierce electrodes are derived for an accelerating system with current density, limited either by space charge or by emitting property of the cathode. As an example of general approach, Pierce electrodes shape is analyzed for a system consisting of two accelerating gaps. It is shown that Pierce's solution exists if the potential U_2 of the second anode does not exceed the potential U_1 of the first accelerating electrode by more than a factor that for space-charge-limited system is equal to $(d_2/d_1 + 1)^{4/3}$, where d_1 and d_2 are the widths of the first and second gaps, respectively. In the opposite case, $U_2/U_1 \geqslant (d_2/d_1 + 1)^{4/3}$, precise solution can hardly be implemented in actual devices but it can still be used as a hint or even as trial function for numerical search of quasi-Pierce electrodes. Based on numerical simulations, guidelines for the design of focusing electrodes are given for the case when Pierce's solution does not exist.

В.И. Давыденко, А.А. Иванов, И.А. Котельников, М.А. Тиунов

Пирсовские электроды для многоступенчатой ускоряющей системы

Аннотация

Известное решение Пирса [1, 2], позволяющее найти форму электродов на границе плоского диода, которая минимизирует угловую расходимость пучка заряженных частиц, обобщено на случай системы, состоящей из нескольких ускоряющих зазоров. Получены простые формулы, описывающие форму пирсовских электродов в параметрическом виде в ускоряющей структуре с током, ограниченным либо пространственным зарядом, либо эмиссией катода. В качестве примера реализации общего подхода исследована форма пирсовских электродов в системе, состоящей из двух ускоряющих промежутков. Показано, что решение Пирса существует, если потенциал второго ускоряющего электрода U_2 не превышает потенциал первого ускоряющего электрода U_1 более чем на некоторый множитель, который в случае тока, ограниченного пространственным зарядом, равен $(d_2/d_1 + 1)^{4/3}$, где d_1 и d_2 – толщина первого и второго ускоряющих промежутков, соответственно. В противоположном случае, когда $U_2/U_1 \geqslant (d_2/d_1 + 1)^{4/3}$, точное решение технически трудно реализовать в реальных устройствах, однако его можно использовать в качестве ориентира при численном поиске электродов с формой, близкой к пирсовской. На основе соответствующего численного анализа даны рекомендации по выбору геометрии фокусирующих электродов для случая, когда решение Пирса не существует.

1 Introduction

Pierce electrode is an important part of many electron and ion guns. For a space-charge dominated gun, the shaped electrodes serve to establish correct potential variation along the beam boundary. The analytic derivation by J.R. Pierce [1, 2] gives shape of the electrodes outside the beam aperture that sustains the potential profile within the beam interior as it would be in an infinite planar diode which obeys the Child-Langmuir law.

In our previous papers [3, 4], we have extended Pierce's solution to a multigap accelerating system, where the current density is limited by space charge. In this paper we extend this treatment to a more general case, where the current density can be limited also by the emitting property of the cathode. Bearing in mind adaptation of general theory to production of precise ion beams, which can be used, for example, for plasma diagnostics [5], we consider an unit consisting of two planar gaps as the most simple example. As was shown in [3, 4], Pierce-like solution in multigap systems exists only if acceleration rate in second gap is, in a sense, smaller that in the first gap. On the contrary, most commonly used design of multigap systems adopts higher acceleration rate in the second and in the following gaps. In this paper, we analyze this regime in more details and show that shaping some of the electrodes according to Pierce-like solution still allows to diminish emittence of the beam though it is not possible to use Pierce-like shapes for all the electrodes at once.

2 Child-Langmuir problem

Let us consider an accelerating system consisting of two plane gaps as shown in Fig.1. The emitting electrode (cathode) is placed at the plane z=0, first and second accelerating electrodes (first and second anodes)

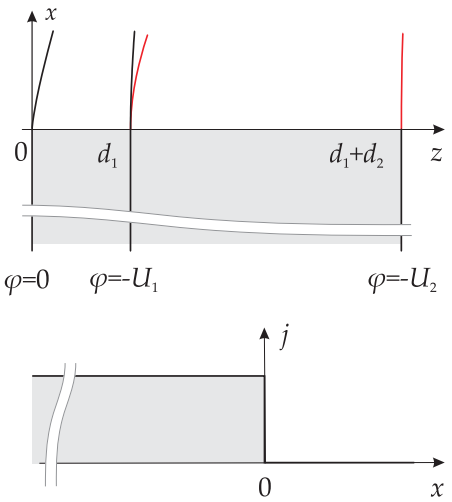

Figure 1: Schematic view of a planar diode with the steep current density profile. Pierce electrodes outside the beam aperture, in the half-space $x > 0$, compensate transversal electric field at the beam edge so that $E_x = 0$ within the entire region $x \leqslant 0$, occupied by the beam.

are placed at $z = d_1$ and $z = d_2 + d_1$. The three electrodes have the potentials $\varphi = 0$, $\varphi = -U_1$, and $\varphi = -U_2$, respectively.

We neglect thermal spread of ion distribution as it is usually done in simplified theories. Then the ion density n and the current density j are related by the hydrodynamic equation

$$j = en\sqrt{-2e\varphi/m}. \tag{1}$$

Finite ion temperature imposes lower limit on local angular divergence, which can not be eliminated by Pierce electrodes. Evaluating n from (2) and substituting it into the 1D version of the Poison's equation

$$\frac{d^2\varphi}{dz^2} = -4\pi en \tag{2}$$

leads to an ordinary differential equation which describes particle flow in a planar diode with somehow compensated transverse electric field at

the periphery. The equation should be supplemented with the boundary conditions

$$\frac{d\varphi}{dz} = -E_0, \tag{3a}$$

$$\varphi = 0 \tag{3b}$$

at $z = 0$,

$$\varphi = -U_1 \tag{3c}$$

at $z = d_1$, and

$$\varphi = -U_2 \tag{3d}$$

at $z = d_1 + d_2$. For a given electric field E_0 at the first emitting electrode the system (1)–(3b) yields the density j of electric current through the diode. Alternatively, for a given j it allows to find E_0 but the latter problem has no physical solution if j exceeds the current density through the charge limited diode as predicted by the Child-Langmuir law

$$j_{\mathrm{CL}} = \frac{1}{9\pi d_1^2}\sqrt{\frac{2eU_1{}^3}{m}},$$

that corresponds to $E_0 = 0$.

Henceforth the current density j is measured in units of j_{CL}, the coordinate z in units of the width d_1 of the first gap, the potential φ in units of the voltage $\varphi(d_1) = -U_1$ at the first anode, and the electric field E in terms of U_1/d_1. It means that dimensionless electric field is related to dimensionless electric potential by the equation $E = d\varphi/dz$ (without minus sign), so that both E and φ are positive in an accelerating system. Chosen way of normalization is suitable both for ion and electron guns since eU_1^3 must be positive for the particles of given charge e to be accelerated by given potential $-U_1$ at the first anode.

In normalized units, Poisson's equation (2) reads

$$\varphi'' = \frac{4}{9}\,\frac{j}{\sqrt{\varphi}}\,, \tag{4}$$

where the prime stands for the derivative over z. Integrating eq. (4) once over z yields the first integral:

$$(\varphi')^2 = \frac{16j}{9}\,[\sqrt{\varphi} + \alpha]\,, \tag{5}$$

where α is a constant to be found from the boundary conditions separately for the first and second gaps. As to the current density j, we assume that it is the same in both gaps, and net current to the 1st anode is absent. Henceforth we shall use the indices 1 and 2 to distinguish the parameters and functions related to the 1st and 2nd gaps, respectively.

2.1 First gap

Since $\varphi_1 = 0$ at $z = 0$, we conclude that

$$\alpha_1 = 9E_0^2/16j \tag{6}$$

within 1st gap. Integrating positive root $\varphi' > 0$ of eq. (5) with the boundary condition (3c), one obtains the equation

$$2\alpha_1^{3/2} + (\sqrt{\varphi_1} - 2\alpha_1)\sqrt{\alpha_1 + \sqrt{\varphi_1}} = \sqrt{j}\,z. \tag{7}$$

Together with the boundary condition $\varphi_1 = 1$ at $z = 1$ it gives the dependence j on the parameter α_1:

$$j(\alpha_1) = \left[2\alpha_1^{3/2} + (1 - 2\alpha_1)\sqrt{1 + \alpha_1}\right]^2. \tag{8}$$

Then eq. (6) relates E_0 with α_1:

$$E_0(\alpha_1) = \frac{4}{3}\sqrt{j(\alpha_1)\alpha_1} = \frac{4}{3}\,\sqrt{\alpha_1}\left[2\alpha_1^{3/2} + (1 - 2\alpha_1)\sqrt{1 + \alpha_1}\right]. \tag{9}$$

The parameter α_1 varies from $\alpha_1 = 0$, when $E_0 = 0$ and $j = 1$, to $\alpha_1 = \infty$, when $E_0 = 1$ and $j = 0$, providing parametric representation of the dependence j on E_0 through eqs. (8) and (9) as shown in Fig. 2. The parameter α_1 can be eliminated from eqs. (8) and (9) to give

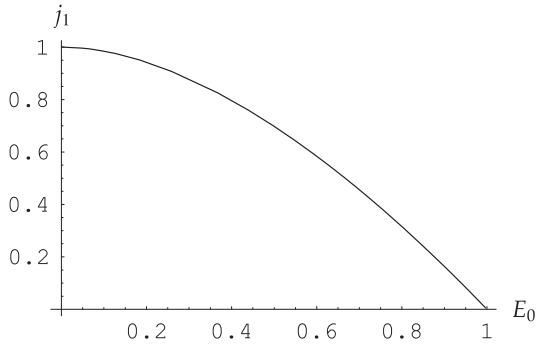

Figure 2: Plot $j(E_0)$.

explicit dependence j on E_0:

$$j(E_0) = \frac{1}{2}\left(1 \pm \sqrt{1 - \frac{27}{4}E_0^2 + \frac{27}{4}(E_0^2)^{3/2}}\right).$$

However the explicit form is less convenient since it is multivalued function with two branches, which intersect at $E_0 = 2/3$. The plus signs in r.h.s. of the last equation is to be taken if $E_0 < 2/3$, and the minus sign is suitable for the case $E_0 > 2/3$.

For a given parameter α_1 eq. (7) together with eq. (8) implicitly give the potential φ_1 as a function of z:

$$z = \frac{2\alpha_1^{3/2} + (\sqrt{\varphi_1} - 2\alpha_1)\sqrt{\alpha_1 + \sqrt{\varphi_1}}}{2\alpha_1^{3/2} + (1 - 2\alpha_1)\sqrt{\alpha_1 + 1}}. \tag{10}$$

Eq. (10) is cubic in respect to $\sqrt{\alpha_1 + \sqrt{\varphi_1}}$. Generally, cubic equation with real coefficients may have one or three real roots for given values of α_1 and z. Two additional roots can merge merely at $\varphi_1 = 0$; to prove this, one needs to note that the derivative of r.h.s. of eq. (10) over $\sqrt{\alpha_1 + \sqrt{\varphi_1}}$ is equal to zero at the merging point. Inserting $\varphi_1 = 0$ into r.h.s. of eq. (10) makes it equal to 0. It means that $\varphi_1(z)$ has merely one real branch within the entire first gap. In particular case

$\alpha_1 = 0$, corresponding to Child-Langmuir law, eq. (10) yields

$$\varphi_1(z) = z^{4/3} \tag{11}$$

for the region $0 < z < 1$. If $\alpha_1 \to \infty$, eq. (10) reduces to $\varphi_1(z) = z$ since $j \to 0$ and space charge becomes negligibly small.

2.2 Second gap

Applying the equation (5) to 2nd gap, one can deduce that

$$\alpha_2 = 9E_{1+}^2/16j - 1, \tag{12}$$

where E_{1+} is the electric field at $z = 1$ in the 2nd gap. Since $j > 0$, the parameter α_2 can vary from -1 to positive infinity, i. e. $\alpha_2 > -1$. Similarly, the parameter α_1 can be expressed through the electric field E_{1-} at the first anode from the side of 1st gap:

$$\alpha_1 = 9E_{1-}^2/16j - 1. \tag{13}$$

It is readily seen therefore that the difference of the parameter α_2 from α_1 is related to the surface charge $\sigma = (E_{1+} - E_{1-})/4\pi$ at the the first anode. Hence, $E_{1+} > E_{1-}$ if $\alpha_2 > \alpha_1$, and $\alpha_2 < \alpha_1$ if $E_{1+} < E_{1-}$.

Taking a positive root $\varphi' > 0$ of eq. (5) with $\alpha = \alpha_2$ and integrating resulting equation with the boundary condition (3c) yields the equation

$$z = 1 + \frac{(2\alpha_2 - 1)\sqrt{\alpha_2 + 1} + \left(\sqrt{\varphi_2} - 2\alpha_2\right)\sqrt{\alpha_2 + \sqrt{\varphi_2}}}{\sqrt{j}}, \tag{14}$$

which implicitly determines the potential in the 2nd gap. Being essentially cubic equation in respect to $\sqrt{\sqrt{\varphi}_2 + \alpha_2}$, it has three distinct roots, but two of them are complex (i. e., nonphysical) or do not obey the boundary conditions. Indeed, one can readily show that two real roots merge at the point

$$z_m = 1 + \frac{(2\alpha_2 - 1)\sqrt{\alpha_2 + 1} - 2\alpha_2^{3/2}}{\sqrt{j}},$$

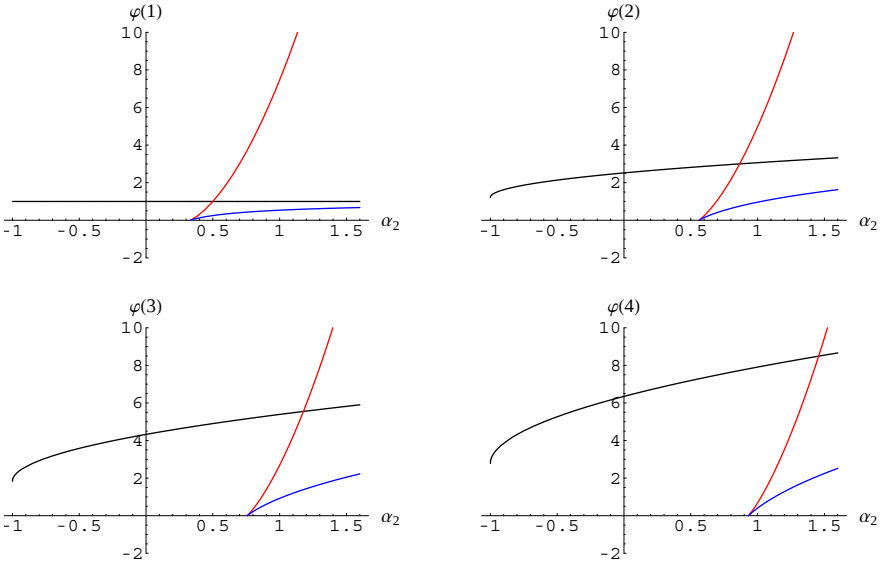

Figure 3: Real roots of eq. (14) for $j = 1$ at $z = 1$ (top, left), $z = 2$ (top, right), $z = 3$ (bottom, left), $z = 4$ (bottom, right). If $\varphi_2(z;1)$ is the potential in the second gap for the case $j = 1$, then the scaled function $\varphi_2(z;j) = \varphi_2(1+(z-1)\sqrt{j};1)$ gives the potential for a smaller current density $j < 1$.

where they have the magnitude $\varphi_2 = 0$. Since $z_m > 1$ for any admissable values of α_2 and j, only one of the roots satisfies the boundary condition (3c) at $z = 1$. Fig. 3 shows the dependence of all real roots on α_2 for successively growing coordinate z.

Together with the boundary condition (3d) eq. (14) relates α_2 to α_1:

$$d_2 = \frac{(2\alpha_2 - 1)\sqrt{\alpha_2 + 1} + \left(\sqrt{U_2} - 2\alpha_2\right)\sqrt{\alpha_2 + \sqrt{U_2}}}{2\alpha_1^{3/2} + (1 - 2\alpha_1)\sqrt{\alpha_1 + 1}}\,. \qquad (15)$$

Physically feasible values of α_2 grow as U_2 becomes larger. It is seen from (15) that $U_2 = (1 + \sqrt{j}\,d_2)^{4/3}$ if $\alpha_2 = 0$; $\alpha_2 > 0$ for larger U_2. As an example, real branches of $\varphi_2(z)$ are shown in Fig. 4 for four values of $\alpha_2 = -1$, 0, 0.5 and 1; if $d_2 = 3$, these values correspond

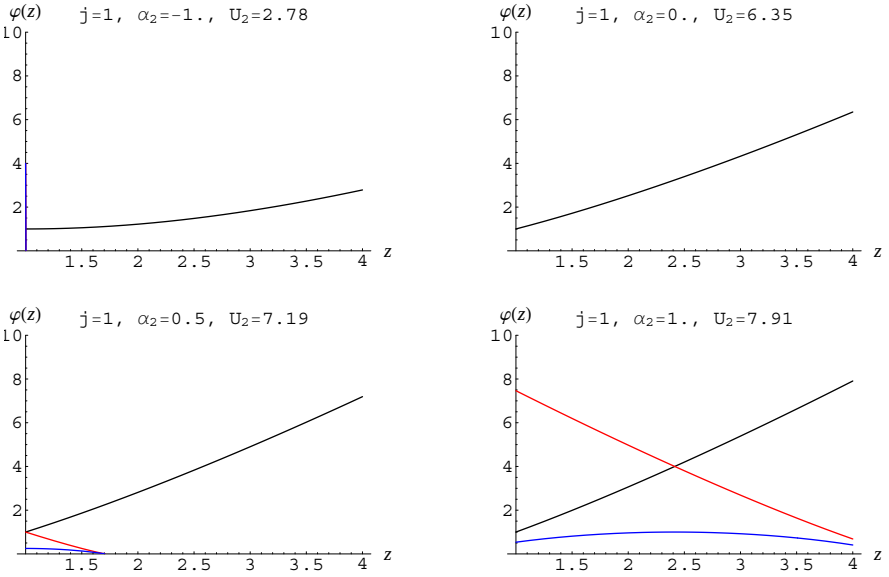

Figure 4: Real roots of eq. (14) for $j = 1$ at $\alpha_2 = -1$ (top left), $\alpha_2 = 0$ (top right), $\alpha_2 = 0.5$ (bottom left), $\alpha_2 = 1$ (bottom right). Electric potential for smaller current density can be expressed through $\varphi_2(z;1)$ at $j = 1$ as $\varphi_2(z;j) = \varphi_2(1 + (z-1)\sqrt{j};1)$.

to $U_2 = 2.78$, 6.35, 7.19 and 7.91 (recall that we use dimensionless variables such that $d_1 = 1$, $U_1 = 1$).

3 Pierce electrodes

The equations (10) and (14) provide a solution to 1D problem where particle flow is unbounded in any direction across the direction of the beam. Space charge of a beam, limited in transverse direction, inevitably creates transverse electric field that increases angular divergence of the flux. The transverse field can be compensated by a special geometry of additional electrodes placed outside the beam. J.R. Pierce [1, 2] showed that the shape of such electrodes can be found by means of analytic continuation of the 1D solution.

Let $x = 0$ be the plane boundary of the ion flux that occupies the half-space $x < 0$, where the potential $\varphi(z)$ is given by the equation (10) or (14) for the first or for the second gaps respectively. The opposite half-space $x > 0$ is empty. Then the function

$$\psi(x, z) = \tfrac{1}{2}\left[\varphi(z + ix) + \varphi(z - ix)\right] \tag{16}$$

obeys Laplace equation

$$\Delta\psi = \frac{\partial^2\psi}{\partial x^2} + \frac{\partial^2\psi}{\partial z^2} = 0 \tag{17}$$

in the empty region. The function ψ is continuous at the boundary of the beam, $\psi(0, z) = \varphi(z)$, and provides the continuity of the transverse electric field since $\partial\psi(0, z)/\partial x = 0$. The equipotential surfaces $\psi(x, z) = \text{const}$ give the shape of conducting electrodes that can provide required space distribution of potential $\psi(x, z)$ at the beam's boundary.

To find the shape of the equipotential surfaces in empty region it is sufficient to replace z by $z + ix$ and insert $\psi + is$ instead of φ_1 or φ_2 respectively in eq. (10) or (14). Separating real and imaginary parts of these equations then yields the functions $x(\psi, s)$ and $z(\psi, s)$. The parts describe the shape of equipotential surfaces with prescribed potential ψ while the parameter s runs from zero at the edge of the beam to positive infinity at $x \to \infty$. On the contrary, for a fixed parameter s and varying ψ, these functions give parametric presentation of the electric force lines. Specifically,

$$z + ix = 1 + \frac{2\alpha_1^{3/2} + (\sqrt{\psi + is} - 2\alpha_1)\sqrt{\alpha_1 + \sqrt{\psi + is}}}{2\alpha_1^{3/2} + (1 - 2\alpha_1)\sqrt{\alpha_1 + 1}} \tag{18}$$

in the continuation region that matches 1st gap. Pierce electrode that touches the cathode is given by $\psi = 0$, and the opposite electrode is given by $\psi = 1$. The shape of Pierce electrodes that touch first and second anodes from the side of 2nd gap are obtained by equating ψ to

1 and U_2 in

$$z + ix = 1 + \frac{(2\alpha_2 - 1)\sqrt{\alpha_2 + 1} + \left(\sqrt{\psi + is} - 2\alpha_2\right)\sqrt{\alpha_2 + \sqrt{\psi + is}}}{2\alpha_1^{3/2} + (1 - 2\alpha_1)\sqrt{\alpha_1 + 1}}. \tag{19}$$

The two continuation regions, coming from neighboring gaps, overlap, if $\alpha_2 > \alpha_1$. Overlapping of neighboring regions means that Pierce electrode matching first anode can not be actually inserted. In other words, Pierce solution exists if

$$\alpha_2 < \alpha_1. \tag{20}$$

As noted in Sec. 2.2, this occurs if $E_{1+} < E_{1-}$. In particular case, when the current density is limited by the space charge in the first gap, i. e. $j = 1$, the inequality (20) is equivalent to

$$U_2/U_1 < (d_2/d_1 + 1)^{4/3}. \tag{21}$$

Shape of Pierce electrodes is shown in Fig. 5 for the space-charge-limited diode, $j = 1$, and also for the same diode with current density reduced by a half, $j = 0.5$. Facing surfaces of Pierce electrodes are shown by lines with long dashes for the case $j = 1$, and short dashes are used for the case $j = 0.5$. Chain curves (dashes alternating with dots) designate left electrodes, while dashed lines show right electrodes.

Fig. 5,a illustrates the case, when insertion of Pierce electrode to first anode is possible both for $j = 1$ and $j = 0.5$. In this case, left boundary of the continuation region, matching second gap, goes to the right of the right boundary of the continuation region that matches first gap, i.e., chain line, matching the point $x = 0$, $z = 1$, goes to the right from dashed line with dashes of same length.

In Fig. 5,b, intermediate Pierce electrode becomes thinner; for $j = 1$ this electrode shrinks to zero width since both α_2 and α_1 are equal to zero while still $\alpha_2 < \alpha_1 =$ for $j = 0.5$.

In Fig. 5,c, Pierce electrode for the case $j = 0.5$ also shrinks to zero width as $\alpha_2 = \alpha_1 = 0.5$. As to the case $j = 1$, intermediate electrode can not be inserted at all since chain line that touches first anode goes to the left from dashed line.

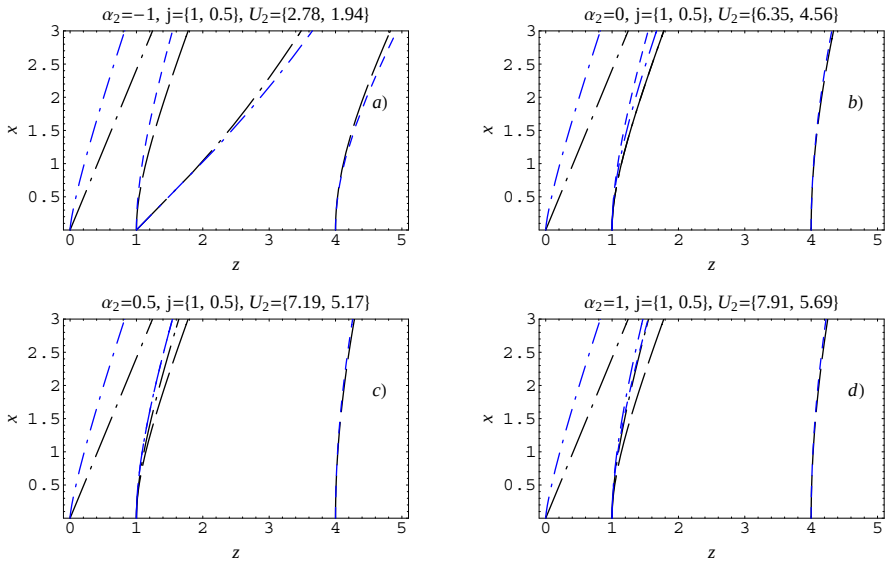

Figure 5: Pierce electrodes: long dashes—$j = 1$, $\alpha_1 = 0$, short dashes—$j = 0.5$, $\alpha_1 = 0.5$; dashed and chain lines designate the electrodes respectively on the left and on the right of corresponding gap; a) $\alpha_2 = -1$, $U_2 = 2.78$ for $j = 1$ and $U_2 = 1.94$ for $j = 0.5$; b) $\alpha_2 = 0$, $U_2 = 6.35$ and $U_2 = 4.56$; c) $\alpha_2 = 0.5$, $U_2 = 7.19$ and $U_2 = 5.17$; d) $\alpha_2 = 1$, $U_2 = 7.91$ and $U_2 = 5.69$. For a given value of the parameter α_2 and the width of the gap $d_2 = 3$, voltage at the second anode U_2 decreases as j becomes smaller.

Finally, in Fig. 5,d, an intermediate Pierce electrode can not be inserted neither for the case $j = 1$ nor for the case $j = 0.5$.

4 Non-equipotential Pierce electrodes

As it was show above, equipotential Pierce electrode can not be adjusted to first anode if $\alpha_2 > \alpha_1$. However it is still possible to use Pierce-like solution for practical design by adjusting non-equipotential electrode as shown in Fig. 6, where joined analytic continuation of the 1D solutions (11) and (14) of the Poisson equation is drawn for $\alpha_1 = 0$,

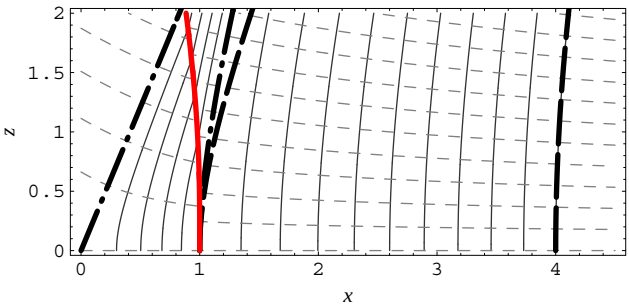

Figure 6: Analytic continuation of (11) and (14) at $\alpha_2 = 1.33$. Contour plot of $\max[\psi_1(x,z), \psi_2(x,z)]$; dashed lines are electric field lines, i. e., contours of $\mathrm{Im}[\varphi(z+ix)]$. Boundaries of analytic continuation ψ_1 and ψ_2, matching respectively 1st and 2nd gaps, are shown by thick dashed and chained lines as explained in Fig. 5. The two continuations overlap. Thick solid line is the matching boundary where $\psi_1 = \psi_2$. Inclination of electric field lines experience a jump at the matching boundary; it means that the boundary bears surface electric charge.

$\alpha_2 = 1.33$, which corresponds to $j = 1$, $U_2 = 25/3$. The analytical continuation $\psi_1(x,z) = \mathrm{Re}[\varphi_1(z+ix)]$ of (11), coming from the segment $0 < z < 1$ of the beam boundary, matches the analytical continuation $\psi_2(x,z) = \mathrm{Re}[\varphi_2(z+ix)]$ of (14), coming from the segment $1 < z < 4$, at the matching surface where $\psi_1(x,z) = \psi_2(x,z)$ shown as thick solid line in Fig. 6.

While the potential shown in Fig. 6 looks as quite smooth, the electric field experience a jump across the matching surface $\psi_1(x,z) = \psi_2(x,z)$. It means that the latter is actually not equipotential and bear a surface charge. From technical point of view, it is hardly possible to construct a structure that would provide prescribed distribution of electrical potential and surface charge along a curvilinear surface. One can speculate, though, that this can be done with the use of a winding, made of a poor conductor and wrapped along the surface. Then a small current, flowing from the anode, could provide desired distribution of potential along the surface. For a given shape of the surface and a given potential distribution along the surface, a desired distribution of the surface charge will be automatically achieved.

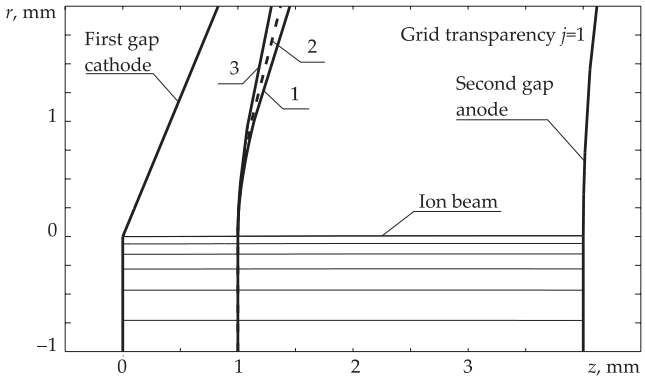

Figure 7: Variants of electrode cuts for various values of hole grid transparency for $j = 1$: 1) intermediate electrode is shaped according to analytical solution for first gap; 2) intermediate electrode is shaped so that it is located in half-way between first and third variants at every distance from the beam edge; 3) intermediate electrode is shaped according to analytical solution for second gap. The shape of all electrodes for the cases $j = 0.75$ and $j = 0.5$ slightly differ from the case $j = 1$ but the difference is hardly distinguishable in the scale of the graph.

5 Computer fit of quasi-pierce electrodes

We used computer code UltraSAM [6] to simulate geometry of electrodes edging near the beam edge in two-gap ion source and to minimize the emittance of the beam in the case $\alpha_2 > \alpha_1$. In this section, the results of computer simulation for a realistic ion source [4] with $d_2 = 3$, $U_2 = 25/3$ are reported.

Of the three electrodes in two-gap-ion-system, merely edging geometry of intermediate electrode (i. e. of the first anode) was varied while that of the first and the third electrodes (i. e. of the cathode and second anode) was kept extremely close to the analytical solution for planar case described above.

Computer simulation was done for three distinct values of the hole grid transparency of the system which correspond to the three values

of the parameter j, namely $j = 1$, $j = 0.75$ and $j = 0.5$. For every value of j, three variants of edging geometry for intermediate electrode were simulated as shown in Fig. 7 that illustrates the case $j = 1$. First variant of the intermediate electrode geometry (the electrode labeled with the numeral 1) is exactly given by analytical solution for the *first gap* of planar ion accelerating system. Third variant corresponds to analytical solution for the *second gap* (numeral 3). Finally, in the second variant (numeral 2) intermediate electrode goes exactly in the midst of the first and the third variants. Since intermediate electrode crosses first electrode at some distance from the beam edge in the second and third variants (recall that the case $\alpha_2 > \alpha_1$ is under consideration in this section), the distance from the edge was limited in this computer simulation to not exceed the sum of the two gaps width, $d_1 + d_2$.

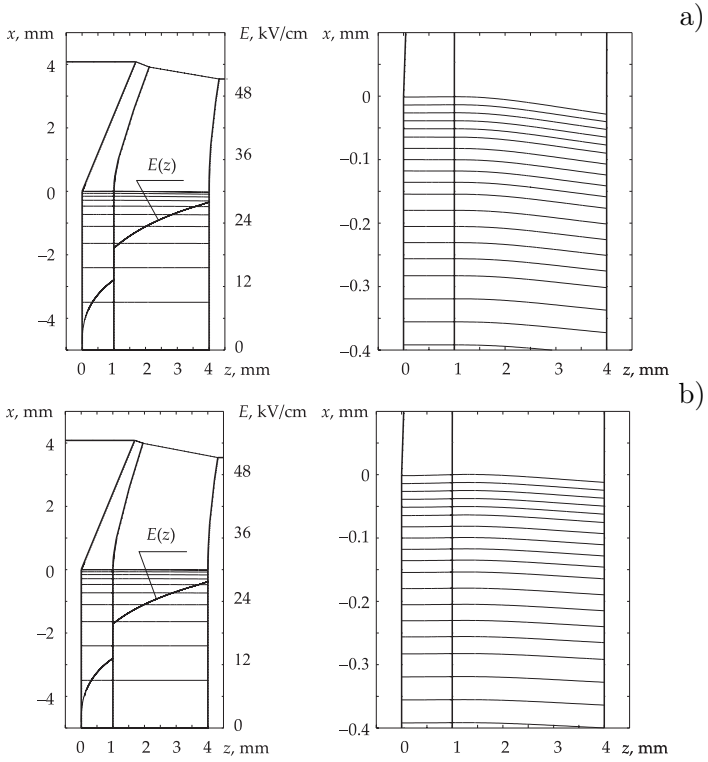

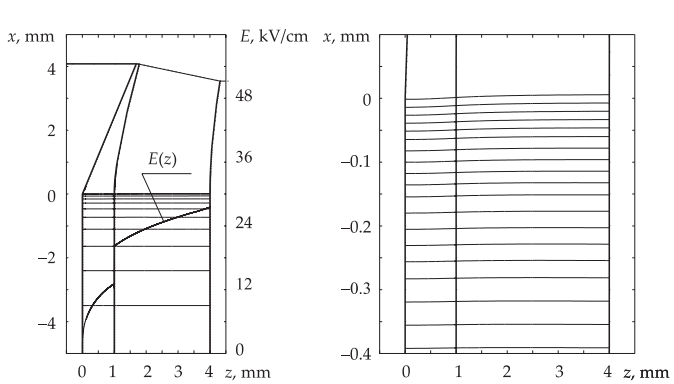

Figure 8: Different edging of two-gaps-ion-gun with maximal transparency of grids, $j = 1$: a) intermediate electrode as anode of first gap; b) intermediate electrode half-way between anode of first gap and cathode of second gap; c) intermediate electrode as cathode of second gap. On the left: geometry of electrodes and longitudinal electric field at the beam edge; on the right: enlarged view of particles trajectories near the beam edge.

Results of computer simulation are presented in Fig. 8 for the case $j = 1$. They show that minimal minimal emittance of the beam is achieved for the shape of the intermediate electrode edging in the third variant, when the electrode acquires analytically calculated shape matching second gap. Corresponding emittance of the edge trajectories for these three variants are shown in Fig. 10,a.

Similar conclusions were made for $j = 0.75$ and $j = 0.5$. Computer simulation certainly show that optimal geometry of intermediate electrode edging corresponds to analytical solution for second gap. Fig. 9 shows optimal geometries of electrode edging for two-gap ion source with $d_2 = 3$ and $U_2 = 25/3$ for reduced transparency of the source grid. Fig. 10,b shows corresponding emittance at the edge of the beam. In all these cases, the angle of deflection of edge trajectories does not exceed one milliradian.

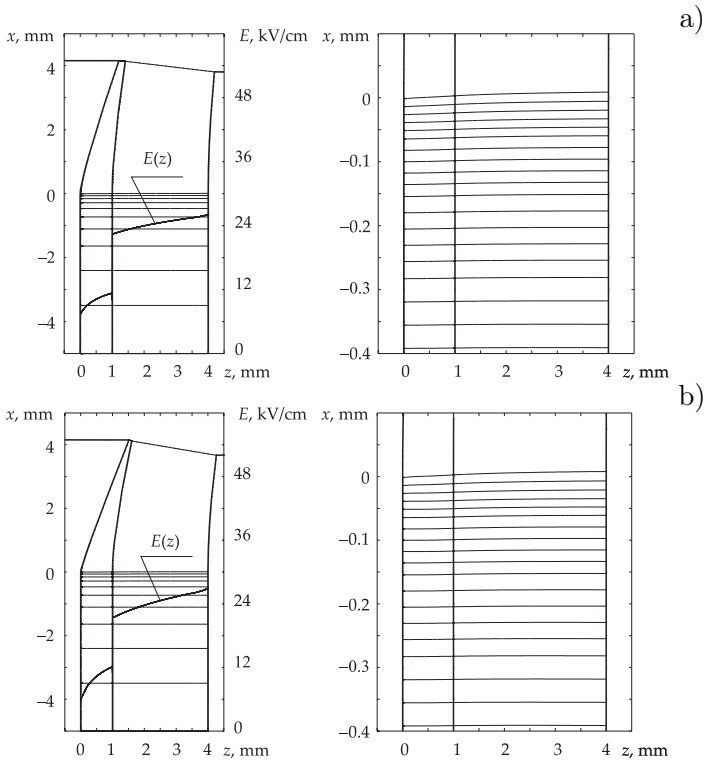

Figure 9: Optimal edging of two-gaps-ion-gun with distinct lower transparency of grids: a) $j = 0.5$; b) $j = 0.75$; c) for the case $j = 1.0$ see Fig. 8,c. Intermediate electrode has shape of Pierce cathode for the second gap.

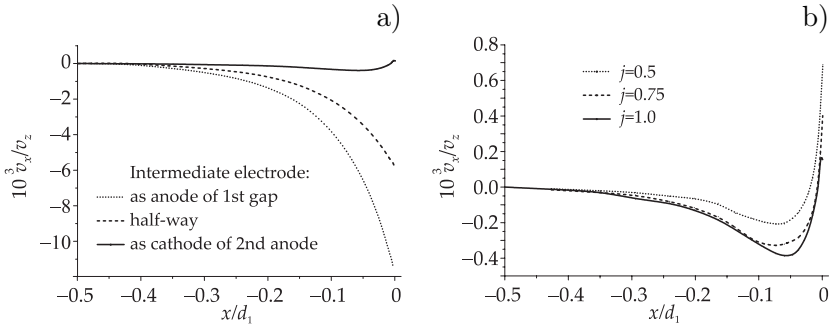

Figure 10: Transverse angle at the edge of the beam: a) different edging of two-gaps-ion-gun with maximal transparency of grids as shown in Fig. 8, b) different grid transparency for optimal edging of two-gaps-ion-gun shown in Fig. 9.

6 Conclusions

In this paper, we adapt an approach, initially developed by J.R. Pierce, to the case of accelerating system with 2 planar gaps. We have shown that external equipotential electrodes can compensate defocusing effect of a spatially limited charged beam providing that the rate of acceleration in the second gap does not exceed the rate of acceleration in a single-gap system of the same total width and the same voltage, namely if $U_2/U_1 \leqslant (d_2/d_1+1)^{4/3}$. We have expressed the shape of compensating electrodes in the parametric form (18) and (19).

To avoid possible misunderstanding, we note that, from practical point of view, unattainability of exact spacial spacial charge effect compensation does not prohibit obtaining well focused beam even if $U_2/U_1 \geqslant (d_2/d_1+1)^{4/3}$. Since the diode perveance grows and, hence, the effect of space charge diminishes as U_2 grows, increasing the voltage on the second gap allows to diminish defocusing effect of the space charge if $U_2/U_1 \gg (d_2/d_1+1)^{4/3}$ despite the fact that exact compensation of the space charge is not possible in this case.

References

[1] *J.R. Pierce.* Rectilinear Flow in Electron Beams. Journ. Appl. Phys., 1940, v. 11, p. 548–554.

[2] *J.R. Pierce.* Theory and Design of Electron Beams. 2nd edition. D. van Nostrand Company, Inc., Toronto—New York–London, 1954.

[3] *V.I. Davydenko, A.A. Ivanov, S.A. Korepanov, I.A. Kotelnikov.* // Int. Conf. on Ion Sources, Caen, France, September 12–16, 2005. Book of abstracts, p.234.

[4] *V.I. Davydenko, A.A. Ivanov, S.A. Korepanov, I.A. Kotelnikov.* // Rev. Sci. Instr. 2006 (to be publsihed).

[5] *V.I. Davydenko, et. al.* // Rev. Sci. Instr., **68**, No.3, p.1418 (1997).

[6] *A.V. Ivanov, M.A. Tiunov.* "UltraSAM — 2D Code for Simulation of Electron Guns with Ultra High Precision", Proceeding of EPAC 2002, Paris, pp.1634–1636, 2002.

V.I. Davydenko, A.A. Ivanov, I.A. Kotelnikov, M.A. Tiunov

Pierce electrodes
for a multigap accelerating system

В.И. Давыденко, А.А. Иванов, И.А. Котельников, М.А. Тиунов

Пирсовские электроды
для многоступенчатой ускоряющей системы

ИЯФ 2006-11

Ответственный за выпуск А.М. Кудрявцев
Работа поступила 9.03.2006 г.

Сдано в набор 8.03.2006 г.
Подписано в печать 13.03.2006 г.
Формат бумаги 60×90 1/16 Объем 1.4 печ.л., 1.1 уч.-изд.л.
Тираж 130 экз. Бесплатно. Заказ № 11

Обработано на IBM PC и отпечатано на
ротапринте ИЯФ им. Г.И. Будкера СО РАН
Новосибирск, 630090, пр.академика Лаврентьева, 11.